

Atomic-phase interference devices based on ring-shaped Bose-Einstein condensates: Two ring case

B. P. Anderson,¹ K. Dholakia,² and E. M. Wright^{1,*}

¹*Optical Sciences Center, University of Arizona, Tucson, AZ 85721, USA*

²*School of Physics & Astronomy, University of St. Andrews,
North Haugh, St. Andrews, Fife KY16 9SS, Scotland, UK*

We theoretically investigate the ground-state properties and quantum dynamics of a pair of adjacent ring-shaped Bose-Einstein condensates that are coupled via tunneling. This device, which is the analogue of a symmetric superconducting quantum interference device, is the simplest version of what we term an Atomic-Phase Interference Device (APHID). The two-ring APHID is shown to be sensitive to rotation.

PACS numbers: 03.75.Fi, 03.75.-b

INTRODUCTION

The last few years have witnessed magnificent advances in the preparation, manipulation, and exploration of atomic Bose-Einstein condensates (BECs). These quantum-degenerate systems offer an excellent experimental platform from which to study a multitude of nonlinear matter-wave phenomena including four-wave mixing [1], dark [2] and bright [3] solitons, superfluid vortices [4], and the generation and study of quantized vortices on toroidal atomic traps or rings. In particular, ring-shaped BECs allow for the study of phenomena related to persistent currents and rotational motion, with potential applications to rotation sensing. In this paper, our goal is to take the first theoretical steps in studying Josephson coupling between adjacent ring BECs (as opposed to concentric ring BECs that have been considered previously [5]). In particular, we investigate how quantum tunneling between two condensates trapped in adjacent toroidal traps, formed for example using optical-dipole traps with Laguerre-Gaussian light beams, modifies both the ground state properties and quantum dynamics of the system. The two-ring BEC system is the simplest example of what we refer to as an Atomic-Phase Interference Device (APHID), essentially a neutral-atom analog of a SQUID (Superconducting Quantum Interference Device). The properties of the APHID will be shown to be strongly influenced by the individual phases of the matter-waves in the rings.

The remainder of this paper is organized as follows: In the next section we elucidate the details of the model we use. Following this, we explore the properties of the ground state and first excited state of the system. We then look at the Josephson coupling and the time-dependent solutions, highlighting important considerations due to the effects of rotation, followed by concluding remarks.

BASIC MODEL

The basic model we consider is shown in Fig. 1(a) and comprises two identical ring BECs labeled $j = 1, 2$ which are in close proximity, and the whole system is rotating at an angular frequency ω_R . The close proximity of the rings allows for spatially dependent tunneling between them via mode overlap, meaning that the rings are coupled, allowing Josephson oscillations [6, 7]. Each individual ring may be realized physically using a toroidal trap of high aspect ratio $R = L/\ell_0$ where L is the toroid circumference and ℓ_0 the transverse oscillator length $\ell_0 = \sqrt{\hbar/m\omega_0}$, with ω_0 the frequency of transverse oscillations, assumed to be harmonic. The transverse trap potential is assumed to be symmetric about an axis consisting of a circle on which the trap potential is minimum. The longitudinal (circumferential) motion on each ring can be described approximately by a 1D coordinate $x_j \in [-L/2, L/2]$ obtained by unfolding the ring and applying periodic boundary conditions, as illustrated in Fig. 1(b). Then, at zero temperature the quantum dynamics of an atomic BEC moving on the paired rings may be described by the following coupled Gross-Pitaevskii equations in a reference frame rotating at ω_R : [8, 9, 10, 11]

$$i\hbar \frac{\partial \psi_j}{\partial t} = \hbar\omega_0 \psi_j - \frac{\hbar^2}{2m} \frac{\partial^2 \psi_j}{\partial x^2} - i(-1)^j \frac{\hbar\omega_R L}{2\pi} \frac{\partial \psi_j}{\partial x} + g|\psi_j|^2 \psi_j + \hbar\Omega(x)\psi_{3-j}, \quad (1)$$

where $\psi_j(x, t)$ is the macroscopic wave function for ring $j = 1, 2$ with normalization condition

$$\int_0^L dx (|\psi_1(x, t)|^2 + |\psi_2(x, t)|^2) = N. \quad (2)$$

Here, N is the number of atoms of mass m , $g = 4\pi\hbar^2 a/(2\pi\ell_0^2 m) = 2\hbar\omega_0 a > 0$ is the effective one-dimensional nonlinear coefficient describing repulsive many-body interactions, a being the s-wave scattering length, and $\Omega(x) > 0$, which is chosen real and positive, is the spatially dependent tunneling frequency between

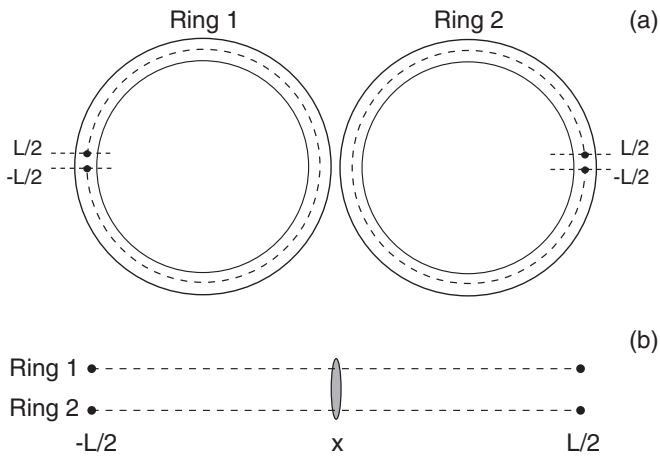


FIG. 1: (a) The basic model we consider comprises two identical ring BECs labeled $j = 1, 2$ which are in close proximity and coupled via tunnelling, and (b) shows the unfolded rings to which periodic boundary conditions are applied. The rings come closest together at the origin $x = 0$, where tunneling is represented by a dark oval.

the two rings. In writing Eqs. (1) we have taken advantage of the fact that although the atoms in each ring are described by different coordinates $x_{j=1,2}$, they can nonetheless be described as moving on the same domain $x \in [-L/2, L/2]$ with the following caveats: First, the atoms on each ring do not cross-interact via mean-field effects, and are only coupled via the spatially dependent tunneling. Second, inspection of Figs. 1(a) and (b) shows that atoms circulating from $x = -L/2 \rightarrow L/2$ along ring $j = 1$ are going counter-clockwise whereas atoms circulating from $x = -L/2 \rightarrow L/2$ along ring $j = 2$ are going clockwise. This means that although we write the equations using a common spatial coordinate $x \in [-L/2, L/2]$, propagation in a given x direction corresponds to opposite senses of rotation for the different rings. This is why the rotation term proportional to ω_R in Eq. (1) has a ring-dependent sign $(-1)^j$.

With reference to Fig. 1(a) we see, for example, that for an atom moving clockwise from a given reference point on ring $j = 1$, then tunnelling over to ring $j = 2$ and moving counter-clockwise, and finally tunnelling back after orbiting ring $j = 2$ to ring $j = 1$ to the original starting point, the atom crosses the tunnelling region twice. In this sense the coupled atomic rings are analogous to a symmetric SQUID [6], in which two superconducting rings are connected by a weak link, which has been employed as a magnetometer [12]. The two ring system, then, is the simplest version of an Atomic-Phase Interference Device, and we concentrate on the two-ring case in this paper to explore the basic properties of APHIDs.

The tunneling frequency $\Omega_{max} = \Omega(x = 0)$ will be at its maximum at the point of closest approach of the rings, which we choose at $x = 0$, and will decrease with

separation, or equivalently as x varies away from the origin. Typically, the tunneling frequency decays exponentially with ring separation. Thus, $\Omega(x)$ will typically be a bell-shaped function of x , and the spatial extent of the Josephson-coupling will be much less than the size of the ring L . Clearly, for smaller rings with tighter curvature, $\Omega(x)$ will drop off faster away from the peak. In the limit $\Omega(x) = 0$, Eqs. (1) reduce to the approximate one-dimensional form previously used to describe atomic BECs on a toroid.

The conserved N-particle energy functional for the coupled Gross-Pitaevskii Eqs. (1) is

$$\begin{aligned}
 E = & N\hbar\omega_0 + \int_0^L dx \left[\frac{\hbar^2}{2m} \left(\left| \frac{\partial\psi_1}{\partial x} \right|^2 + \left| \frac{\partial\psi_2}{\partial x} \right|^2 \right) \right. \\
 & + i \frac{\hbar\omega_R L}{2\pi} \left(\psi_2^* \frac{\partial\psi_1}{\partial x} - \psi_1^* \frac{\partial\psi_2}{\partial x} \right) \\
 & \left. + \frac{g}{2} (|\psi_1|^4 + |\psi_2|^4) + \hbar\Omega(x) (\psi_1\psi_2^* + \psi_1^*\psi_2) \right], \quad (3)
 \end{aligned}$$

giving the energy per particle $\epsilon = E/N$. Since in this paper the transverse confinement energy $\hbar\omega_0$ is assumed the same for both rings and simply redefines the zero of energy, we hereafter drop this energy term for simplicity in notation.

GROUND AND FIRST EXCITED STATES

In this section we examine the properties of the ground and first excited states of a non-rotating ($\omega_R = 0$) pair of coupled ring BECs using a simple model to expose the main features.

Zero-coupling limit

It is useful in assessing the ground state properties to consider the non-coupled case with $\Omega(x) = 0$. If all N atoms are homogeneously distributed on just one of the rings, with $\psi_j = \sqrt{N/L}$ and $\psi_{3-j} = 0$, then according to Eq. (3) the energy per particle is $\epsilon_{trap} = gn/2$, where $n = N/L$ is the linear atomic density. In contrast, when the atoms are equally split between the two rings, but still homogeneously distributed on each ring, $|\psi_j| = \sqrt{N/2L}$, and the energy per particle is

$$\epsilon_{1/2} = \frac{gn}{4}, \quad (4)$$

irrespective of the relative phase between the macroscopic wave functions of the two rings. Energetically speaking then, in the absence of coupling the lowest-energy state is that in which the atoms are equally split between the rings as this minimizes the mean-field energy.

Coupled solutions

To proceed we now re-introduce the coupling and look for solutions where the atoms are equally split between the rings. In particular we consider solutions where the macroscopic wave functions of the two rings are in-phase (+) and out-of-phase (-) by making the ansatz

$$\psi_j(x, t) = \frac{(\pm 1)^j}{\sqrt{2}} e^{-i\mu_{\pm}t/\hbar} \varphi_{\pm}(x), \quad j = 1, 2 \quad (5)$$

with $\varphi_{\pm}(x)$ the mode profiles on each ring and μ_{\pm} the corresponding chemical potentials. Then substituting in Eq. (1) we obtain

$$\mu_{\pm} \varphi_{\pm} = -\frac{\hbar^2}{2m} \frac{d^2 \varphi_{\pm}}{dx^2} + \frac{g}{2} |\varphi_{\pm}|^2 \varphi_{\pm} \pm \hbar \Omega(x) \varphi_{\pm}, \quad (6)$$

and $\int dx |\varphi_{\pm}(x)|^2 = N$. On general grounds, the out-of-phase (-) solution corresponds to the ground state. This can be seen from Eq. (6) where the spatially dependent coupling $\Omega(x) > 0$, which is typically bell-shaped, plays the role of a confining (de-confining) potential for the out-of-phase (in-phase) solution, thereby allowing for lower energy in comparison to the case without coupling.

In the limit $\Omega = 0$ Eq. (6) also has the well-known dark soliton solution [13, 14, 15, 16, 17, 18] on the infinite domain $L \rightarrow \infty$

$$\varphi_{\pm}(x) = \varphi_0(x) = \sqrt{n} \tanh\left(\frac{(x+x_0)}{\sqrt{2}x_h}\right), \quad (7)$$

with $\mu_0 = gn/2$, where n is the linear density of the background (in the thermodynamic limit, where $N \rightarrow \infty$ and $L \rightarrow \infty$, $N/L \rightarrow n$ remains non-zero). The healing length x_h is derived from the relation

$$\frac{\hbar^2}{2mx_h^2} = \frac{gn}{2}. \quad (8)$$

The dark soliton solution represents a flat background density profile with a hole of width $x_h \ll L$ located $x = -x_0$, at which location a phase jump of π also occurs as φ_0 goes through zero. In the thermodynamic limit the energy per particle associated with the dark soliton solution calculated using Eq. (3) is $\epsilon_0 = ng/4 = \epsilon_{1/2}$, that is, it is the same as that in Eq. (4) for a homogeneous density on each ring without coupling. This arises because in the thermodynamic limit $x_h/L \rightarrow 0$, meaning that any energy increase due to the hole in the density makes a negligible effect on average; in other words, the hole in the density occupies a vanishingly small portion of the ring.

Analytic approximation

In general, numerical methods are required to solve Eq. (6) for given parameters and tunneling profile $\Omega(x)$. In

order to obtain insight into the ground-state properties, we employ a simple model

$$\Omega(x) = \Omega_{max} \cdot d \cdot \delta(x), \quad (9)$$

where Ω_{max} is the maximum tunneling frequency and d is the length of the tunneling region. This delta-function approximation will apply when d is much less than any other characteristic length scale of the problem, namely the ring length L and the healing length x_h . For the stationary coupled-ring solutions described by Eq. (6), where $\Omega(x)$ plays the role of a single-particle potential, the delta-function approximation yields a quantum-contact interaction [19]. Substituting Eq. (9) in (6) and integrating from $x = 0_-$ to $x = 0_+$ across the junction, we find that the action of the delta-function coupling is equivalent to a condition on the macroscopic wave function derivative

$$\frac{\hbar^2}{2m} \left(\frac{d\varphi_{\pm}}{dx} \Big|_{x=0_+} - \frac{d\varphi_{\pm}}{dx} \Big|_{x=0_-} \right) = \pm \hbar \Omega_{max} \cdot d \cdot \varphi_{\pm}(0). \quad (10)$$

In the limit $L \gg x_h \gg d$ we further impose the condition that $\varphi_{\pm}(x)$ is symmetric around $x = 0$ in order to satisfy the periodic ring boundary conditions, and we approximate

$$\varphi_{\pm}(x) \approx \sqrt{n} \tanh\left(\frac{(x+x_{\pm})}{\sqrt{2}x_h}\right), \quad x > 0. \quad (11)$$

With this approximation there is a cusp in $\varphi_{\pm}(x)$ at $x=0$, and the solution is extended to $x < 0$ by imposing reflection symmetry around the origin. We can solve for the variables x_{\pm} by substituting the approximate solution (11) in the boundary condition (10), which yields

$$\pm \hbar \Omega_{max} \cdot d = \left(\frac{\hbar^2}{m\sqrt{2}x_h} \right) \frac{[1 - \tanh^2(x_{\pm}/\sqrt{2}x_h)]}{\tanh(x_{\pm}/\sqrt{2}x_h)}. \quad (12)$$

Since $\Omega_{max} > 0$ we find by inspection that the in-phase solutions correspond to $x_+ > 0$ and the out-of-phase solutions to $x_- < 0$. By introducing a dimensionless parameter $\zeta = x_+/\sqrt{2}x_h$, with $\zeta > 0$ and $\zeta = x_-/\sqrt{2}x_h$, with $\zeta < 0$, and using Eq. (8) for the healing length, we may write the above equation as

$$\frac{\hbar \Omega_{max} \cdot d}{g} = \sqrt{\frac{n}{2n_s}} \frac{[1 - \tanh^2(\zeta)]}{\tanh(|\zeta|)}, \quad (13)$$

where $n_s = mg/\hbar^2$ is a scaled density. Figure 2 shows a plot ζ versus the scaled tunneling frequency $\hbar \Omega_{max} \cdot d/g$ for $n/n_s = 10^4$. Figure 3 shows examples of scaled density profiles $|\varphi_{\pm}|^2/n$ for $\hbar \Omega_{max} \cdot d/g = 95$, $\zeta = 0.5$ (solid lines), $\hbar \Omega_{max} \cdot d/g = 6.3$, $\zeta = 2$ (dashed lines) and (a) the out-of-phase or ground-state solution, and (b) the in-phase solution. Density cusps in the solutions are evident, though we note that the ground-state density does not extend down to zero. The key features of the

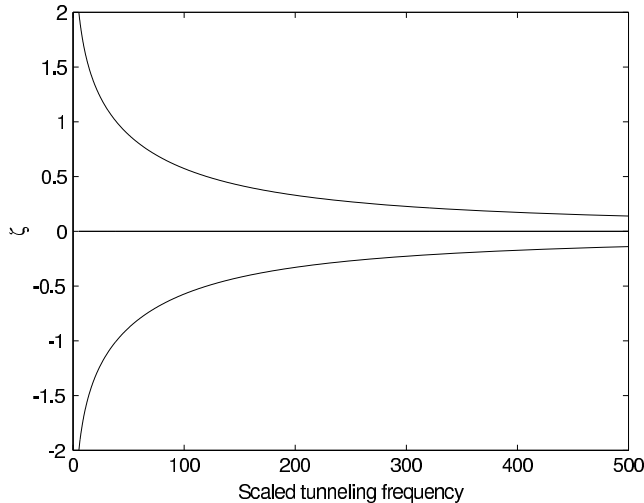


FIG. 2: Plot of ζ versus $\hbar\Omega_{max} \cdot d/g$ for $n/n_s = 10^4$, with $\zeta = x_+/\sqrt{2}x_h, \zeta > 0$ and $\zeta = x_-/\sqrt{2}x_h, \zeta < 0$.

ground state are that as the scaled tunneling frequency $\hbar\Omega_{max} \cdot d/g$ is increased the depth of the density profile increases, the density at the origin going to zero as $\hbar\Omega_{max} \cdot d/g \rightarrow \infty$, and the width of the density hole also increases, approaching x_h as $\hbar\Omega_{max} \cdot d/g \rightarrow \infty$. The in-phase solution is different in that it displays two density zeros and an on-axis maximum that is a cusp, shown in Fig. 3(b). Furthermore, inspection of the in-phase solution shows that its sign reverses through each density zero, and there are two sign reversals around each ring to ensure that the wave functions are single-valued. The in-phase solution therefore has a phase structure like a pair of dark solitons on each ring. For small $\hbar\Omega_{max} \cdot d/g \ll 1$, the density zeros are far apart (dashed line in Fig. 3(b)) for $\hbar\Omega_{max} \cdot d/g = 0.2, \zeta = 2$, but come together at the origin as $\hbar\Omega_{max} \cdot d/g \rightarrow \infty$ (solid line in Fig. 3(b) for $\hbar\Omega_{max} \cdot d/g = 3, \zeta = 0.5$). Thus, for both the in-phase and out-of-phase solutions the density vanishes at the origin as $\hbar\Omega_{max} \cdot d/g \rightarrow \infty$, and we have

$$\varphi_{\pm}(x) \approx \sqrt{n} \tanh\left(\frac{x}{\sqrt{2}x_h}\right). \quad (14)$$

A quantity of physical interest here is the energy per particle ϵ_{\pm} for the two solutions. Using the above approximate solution in the energy functional (3) we find in the thermodynamic limit

$$\epsilon_{\pm} = \frac{ng}{4} \pm \hbar\Omega_{max} \cdot d \cdot n \tanh^2(|\zeta|), \quad (15)$$

where the solution is again parameterized by ζ . Note that in the limit of zero coupling $\Omega_{max} \rightarrow 0$, the energies per particle of the two solutions become the same and equal to that of the equally split solution $\epsilon_{1/2} = ng/4$ as

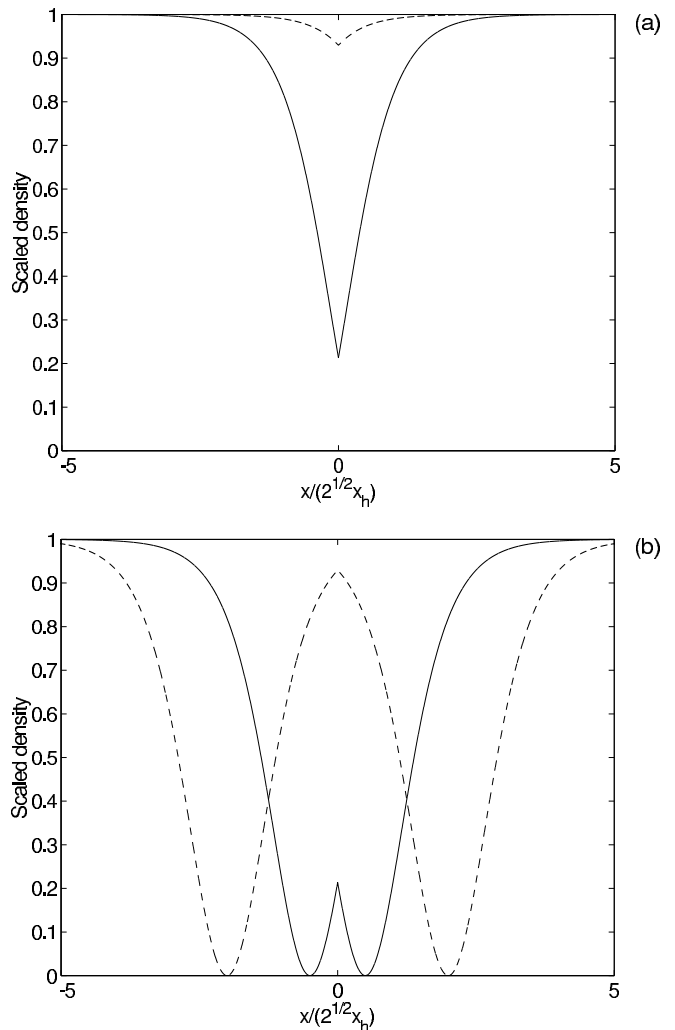


FIG. 3: Scaled density profiles $|\varphi_{\pm}|^2/n$ for $n/n_s = 10^4$, $\hbar\Omega_{max} \cdot d/g = 95, \zeta = 0.5$ (solid lines), $\hbar\Omega_{max} \cdot d/g = 6.3, \zeta = 2$ (dashed lines) and (a) the out-of-phase or ground state solution, and (b) the in-phase solution.

they should. Using Eq. (13) in (15) we obtain finally

$$\epsilon_{\pm} = \epsilon_{1/2} \left(1 \pm \sqrt{\frac{8n}{n_s}} \tanh(|\zeta|)[1 - \tanh^2(\zeta)]\right), \quad (16)$$

which is once again parameterized by ζ . Figure 4 shows $\epsilon_{\pm}/\epsilon_{1/2}$ versus $\hbar\Omega_{max} \cdot d/g$ for $n/n_s = 10$, the upper solid line corresponding to the in-phase (+) solution and the lower solid line to the out-of-phase (-) or ground state solution. For small values of the scaled tunneling frequency $\hbar\Omega_{max} \cdot d/g < 1$ the energy per particle for the in-phase (out-of-phase) solution initially increases (decreases) away from $\epsilon_{1/2}$ for zero-coupling, and this is expected physically. However, as the scaled tunneling frequency is increased further the energy per particle for the in-phase (out-of-phase) solution reaches a turning point at $\hbar\Omega_{max} \cdot d/g \approx 2$, then decreases (increases),

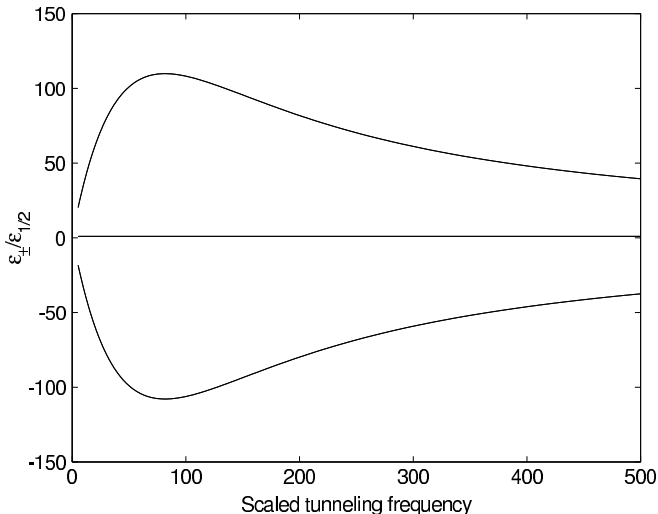


FIG. 4: Scaled energy per particle $\epsilon_{\pm}/\epsilon_{1/2}$ versus $\hbar\Omega_{max} \cdot d/g$ for $n/n_s = 10^4$, the upper solid line corresponding to the in-phase (+) solution and the lower solid line to the out-of-phase (-) or ground-state solution.

and both ϵ_{\pm} tend back to the zero-coupling value $\epsilon_{1/2}$ for $\hbar\Omega_{max} \cdot d/g \rightarrow \infty$. The reason for this is that, as discussed above, for both solutions the density tends to zero at the origin $x = 0$ where the junction is concentrated in the limit $\hbar\Omega_{max} \cdot d/g \rightarrow \infty$, so the Josephson coupling is rendered inoperative and the energy per particle tends to that for zero-coupling.

TIME-DEPENDENT SOLUTIONS

Scaled equations

For purposes of numerical simulations we introduce a simple Gaussian model for the spatially dependent Josephson-coupling

$$\Omega(x) = \Omega_{max} e^{-x^2/w^2} = \Omega_{max} \cdot d \cdot f(x), \quad (17)$$

with Ω_{max} the maximum tunneling frequency and $w \ll L$ the width of the coupling region around $x = 0$. We also introduce the normalized Gaussian $f(x) = \exp(-x^2/w^2)/\sqrt{\pi w^2}$ for which $d = \sqrt{\pi w^2}$ so that effective parameters can be compared with the previous section. Then introducing the scaled variables

$$\tau = t \cdot (ng/\hbar), \quad \xi = x/L, \quad \psi_j = \sqrt{n}\phi_j, \quad (18)$$

with $n = N/L$ the mean density as before, we obtain with $j = 1, 2$,

$$i \frac{\partial \phi_j}{\partial \tau} = -\frac{\beta}{2} \frac{\partial^2 \phi_j}{\partial \xi^2} - i(-1)^j \left(\frac{\nu}{2\pi} \right) \frac{\partial \phi_j}{\partial \xi} + |\phi_j|^2 \phi_j + \eta e^{-\xi^2/\Delta^2} \psi_{3-j}, \quad (19)$$

where $\int d\xi [|\phi_1|^2 + |\phi_2|^2] = 1$, and

$$\Delta = \frac{w}{L} \ll 1, \quad \eta = \frac{\hbar\Omega_{max}}{ng}, \quad \nu = \frac{\hbar\omega_R}{ng}, \quad \beta = \frac{(n/n_s)}{N^2}. \quad (20)$$

These are the scaled equations used for our numerical study. We have solved the equations numerically using the split-step Fast-Fourier transform method [20].

To study the quantum dynamics of coupled-ring BECs we shall use an initial condition at $\tau = 0$ where all N atoms are on one ring in a vortex state of winding number p . This may be realized, for example, by condensing the atoms on one ring in the absence of the other, stirring the BEC to create the vortex [21], and then turning on the second ring. Sauer *et al.* [22] have demonstrated a 2-cm diameter magnetic storage ring for laser-cooled, and Arnold and Riis [23] are working towards realizing a 10 cm diameter magnetically trapped toroidal BEC. One scheme for turning rings off and on is to use toroidal optical dipole traps [24] formed by Laguerre-Gaussian beams piercing a two-dimensional BEC to create the rings [5, 25, 26], or alternatively using scanned laser beams to form the toroidal traps [27]. Cavity field enhancement may also be used to allow for large-radius toroidal traps [28]. Regardless of experimental method, the initial condition we take is

$$\phi_1(\xi, 0) = e^{2\pi i p \xi}, \quad \phi_2 = 0. \quad (21)$$

Resonance conditions

To proceed we examine the resonance conditions leading to the initial exchange of atoms from ring 1 \rightarrow 2 using first-order perturbation theory. For the initial condition (21) we choose the zeroth-order solution as that for $\nu = 0$

$$\phi_1^{(0)}(\xi, \tau) = e^{2\pi i p \xi} e^{-i(2\pi^2 \beta p^2 - p\nu + 1)\tau}. \quad (22)$$

Then writing the first-order solution for ring 2 in the form

$$\phi_2^{(1)}(\xi, \tau) = \sum_{q=-\infty}^{\infty} a_q(\tau) e^{2\pi i q \xi} e^{-i(2\pi^2 \beta q^2 + q\nu)\tau}, \quad (23)$$

yields

$$|a_q(\tau)|^2 = 4\eta^2 \mathcal{F}_{pq}^2 \cdot \frac{\sin^2(\chi_{pq}\tau/2)}{\chi_{pq}^2}, \quad (24)$$

where

$$\mathcal{F}_{pq} = \sqrt{\pi} \Delta e^{-\pi^2 \Delta^2 (p-q)^2}, \\ \chi_{pq} = 2\pi^2 \beta (p^2 - q^2) - \nu(p+q) + 1. \quad (25)$$

The vortex states q of ring 2 are therefore excited and generally exhibit small oscillations except at resonance where χ_{pq} becomes small. The level of excitation of the

q^{th} vortex state is also dictated by the factor \mathcal{F}_{pq} , but since we assume a narrow junction $w/L = \Delta \ll 1$, this factor allows for almost constant excitation $\mathcal{F}_{pq} \approx \sqrt{\pi}\Delta$ in the range $q = p \pm \delta q$ with

$$\delta q = \frac{1}{\pi\Delta} \gg 1. \quad (26)$$

Consider first the case that the system is not rotating $\nu = 0$: Resonance occurs for that integer value of q_r for which χ_{pq} is equal to or closest to zero

$$q_r^2 = p^2 + \frac{1}{2\pi^2\beta}, \quad (27)$$

the width of the resonance being

$$\Delta q \approx \frac{1}{2\pi^2(p + q_r)\beta}. \quad (28)$$

When the width of the resonance is small $\Delta q < 1$ the initial vortex of index p in ring 2 will selectively couple to vortices with mode indices q_r satisfying Eq. (27) in ring 2, giving rise to relatively simple few mode dynamics. In contrast, when $\Delta q \gg 1$ the initial vortex of index p in ring 2 will couple to a broad range of vortices with mode indices $q_r \pm \Delta q$ in ring 2, giving rise to multi-mode dynamics and complex behavior. In addition, for Josephson oscillations to occur the tunneling energy per particle averaged over the ring length $(1/L) \int dx \cdot \hbar\Omega(x) = \hbar\Omega_{max}\sqrt{\pi w}/L$ should be for the same order as the mean-field energy per particle ng , or

$$\eta = \frac{\hbar\Omega_{max}}{ng} \sim \frac{1}{\sqrt{\pi}\Delta}. \quad (29)$$

This gives an estimate of the scaled tunneling frequency η to obtain Josephson oscillations.

Numerical results

Here we present some examples of the dynamics of coupled ring BECs. For all the simulations we set $p = 0, \Delta = 10^{-2}$, and $\eta = 50$. Consider first that the initial state corresponds to the ground state ($p = 0$) of ring 1. From Eqs. (27) and (28) we obtain

$$q_r = \sqrt{\frac{1}{2\pi^2\beta}} = \Delta q, \quad (30)$$

that is, the width of the resonance Δq is equal to the resonant value $q = q_r$. Figure 5(a) shows the fraction of atoms in each ring for $\beta = 1$ for which $q_r = \Delta q = 0.22$, and complete Josephson oscillations between the two rings are evident. In this case the density profiles in the two rings are largely flat as resonant coupling occurs between $p = 0, q_r \approx 0$. In contrast, for $\beta = 5.1 \times 10^{-2}$ as shown in Fig. 5(b) for which $q_r = \Delta q = 1$, the Josephson oscillations are now incomplete. Physically, there are

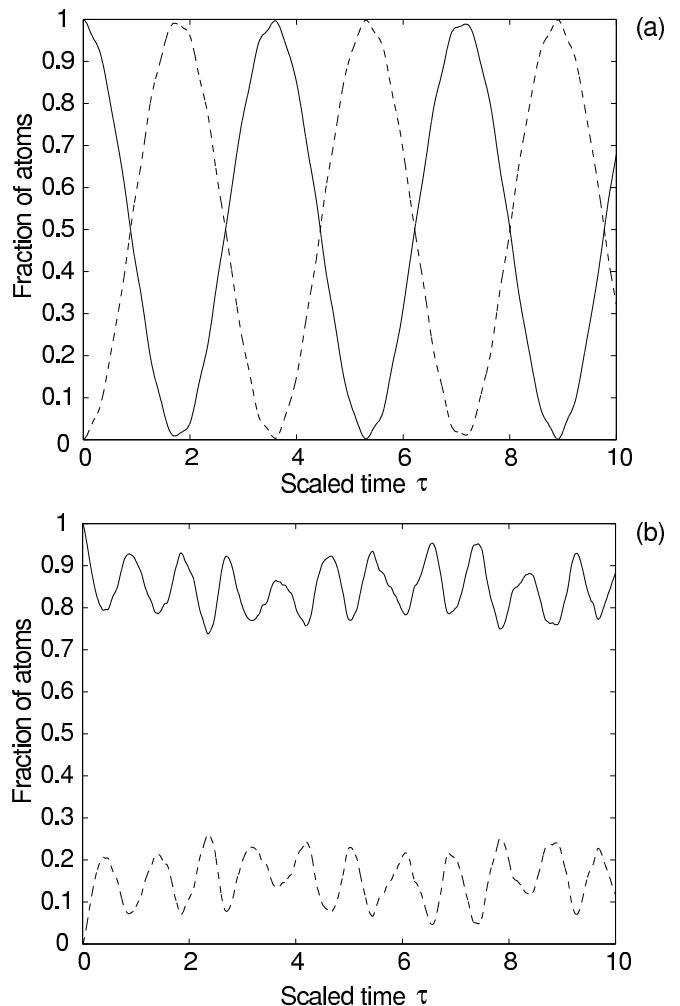


FIG. 5: Fraction of atoms in each ring for $\Delta = 10^{-2}, \eta = 50$, and (a) $\beta = 1, \Delta q = 0.22$, and (b) $\beta = 5.1 \times 10^{-2}, \Delta q = 1$.

multiple modes involved in ring $j = 2$ with $q = 0, \pm 1, \pm 2$, and the resulting multi-mode dynamics is what frustrates the Josephson oscillations for $\Delta q \geq 1$. The multi-mode dynamics manifests itself as spatial density modulations in the two rings as shown in Fig. 6(a) for the same parameters as in Fig. 5(b) and $\tau = 10$. For even lower density $\beta = 5.1 \times 10^{-4}$ for which $q_r = \Delta q = 10$, the Josephson oscillations are all but extinguished, and the spatial density profiles in rings $j = 1, 2$ are shown in Figs. 6(b) for $\tau = 10$. Clearly, the multi-mode nature of the solution allows the coupling due to tunneling to concentrate around the coupling region, hence reducing the net fraction of atoms transferred between the rings.

Some estimates of parameters are in order. Using $g = 2\hbar\omega_0 a$ gives $ng = 2\hbar\omega_0 N(a/L)$, and $\Omega_{max} = 2\eta\omega_0 N(a/L)$. Then for $\omega_0 = 2\pi \times 10^2 \text{ rad}\cdot\text{s}^{-1}, N = 10^3, L = 1 \text{ cm}, a = 5 \text{ nm}$, we find $\Omega_{max} = 2\pi \times 5 \text{ rad}\cdot\text{s}^{-1}$, and τ is time in units of $\hbar/ng = 1.6 \text{ s}$, so the Josephson oscillations in Fig. 5(a) occur on a time scale of seconds. Setting $m = 10^{-25} \text{ kg}$ we obtain $n_s = mg/\hbar^2 \approx 63 \text{ cm}^{-1}$,

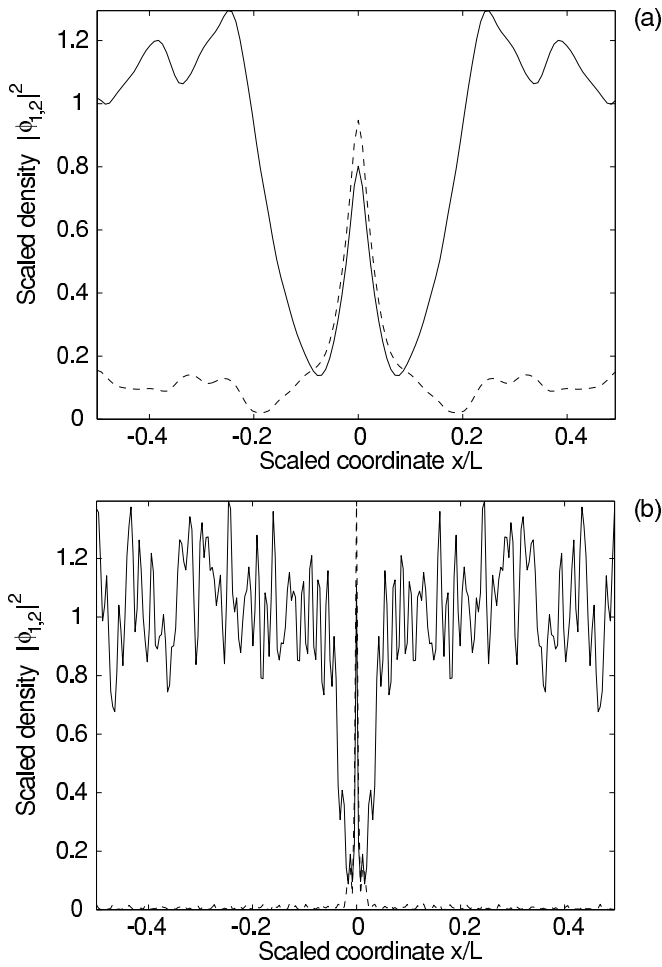


FIG. 6: (a) Spatial density in ring $j = 1$ (solid line) and $j = 2$ (dashed line) for the same parameters as Fig. 5(b) with $\tau = 10$, $\beta = 5.1 \times 10^{-2}$, and $\Delta q = 1$; (b) spatial density in ring $j = 1$ (solid line) and $j = 2$ (dashed line) for $\beta = 5.1 \times 10^{-4}$, $\Delta q = 10$ for $\tau = 10$.

and for $n = N/L = 10^3 \text{ cm}^{-1}$, $\beta = 1.6 \times 10^{-5}$. It is important that $n/n_s > 1$ to ensure that the one-dimensional gas acts as a BEC as opposed to a Tonks gas [29, 30]. The parameter $\beta = (n/n_s)/N^2$ is proportional to $1/\omega_0$ and $1/N$ so we can increase β by decreasing either the number of atoms and/or the transverse oscillator frequency with respect to the above values.

Effects of rotation

An interesting feature of the two ring APHID is that the condition $\chi_{pq} = 2\pi^2\beta(p^2 - q^2) - \nu(p + q) + 1 \rightarrow 0$ for resonant coupling between the rings is dependent on the scaled rotation rate $\nu = \hbar\omega_R/ng$. In particular we find for $p = 0$

$$q_r = \frac{1}{4\pi^2\beta} \left[-\nu \pm \sqrt{\nu^2 + 8\pi^2\beta} \right]. \quad (31)$$

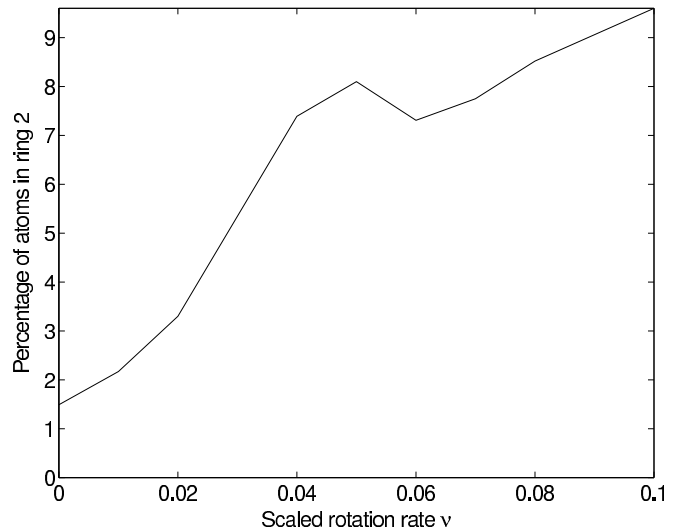


FIG. 7: Percentage of atoms in ring $j = 2$ as a function of scaled rotation rate $\nu = \hbar\omega_R/ng$.

This implies that for scaled rotation rates $|\nu| > \sqrt{8\pi^2\beta}$ the rotation of the entire APHID will affect the coupling. Consider then a case where without rotation $\Delta q \gg 1$ so that the Josephson-oscillations are all but extinguished and the atoms remain on ring 1. Then as the scaled rotation rate ν is increased from zero, inspection shows that one solution q_r in Eq. (31) moves towards resonance while the other moves further away. Therefore, starting from a detuned case with minimal coupling, increased rotation leads to increased coupling which can then be detected via the number of atoms on ring 2 at a fixed detection time. Figure 7 shows the percentage of the atoms in ring 2 versus scaled rotation rate ν at time $\tau = 10$ and $\Delta = 0.01$, $\kappa = 50$, $\beta = 5.1 \times 10^{-4}$, for which $q_r = \Delta q = 10$, and the effect of rotation dependent coupling between the rings is clearly exhibited. Some points are worth making here: First, the rotation causes the number of atoms in ring 2 to change by about 10% of the total number of atoms, so experimentally it will be necessary to control the initial number of atoms on ring 1 to better than this percentage. Furthermore, it would be a challenge to detect the small number of atoms in ring 2. Second, for our particular example with $p = 0$ the number of atoms in ring 2 is sensitive to the magnitude but not the sign of the rotation, but this can be changed by having $p \neq 0$ in which case the the coupling becomes sensitive to the sign of ν . Third, the sensitivity of the atom number to rotation rate increases with the observation time τ chosen, remembering that we are in a far-off-resonant situation so coupling happens slowly. Finally, the number of atoms in ring 2 is not necessarily a monotonic function of the rotation rate, as seen from Fig. 7, which will limit the range of rotation rates that can be uniquely measured. Nonetheless, we feel this is an interesting phenomena which may have utility for rotation

sensing with further development.

To gain some sense of the sensitivity of this scheme we use the same parameters as the previous section for which τ is time in units of $\hbar/ng = 1.6$ s. Then a value of $\nu = 0.01$ corresponds to a rotation rate $\omega_R = 2\nu\omega_0 N(a/L) = 2\pi \times 10^{-3}$ rads $^{-1}$ which is one hundred times higher than the Earth's rotation rate at the poles. However, if we are willing to reduce the transverse oscillator frequency to $\omega_0 = 2\pi \times 1$ rads $^{-1}$, then $\nu = 0.01$ corresponds to the Earth's rotation rate, but then time is in units of 160 s in the figures! We are currently working on schemes involving multiple-ring APHIDs to enhance the rotation sensitivity.

SUMMARY AND CONCLUSIONS

In summary, we have presented a theoretical investigation of a pair of ring BECs coupled by tunneling as the simplest example of a potential Atomic Phase Interference Device. We have shown that the two-ring APHID has interesting ground-state properties, with density profiles reminiscent of dark soliton states around the point of contact of the rings. Furthermore, we have demonstrated that Josephson oscillations between the two rings can occur, and that these oscillations are sensitive to the state of rotation of the APHID. In particular, if all the atoms are prepared on one ring, then the number of atoms transferred to the second ring in a given time span is a measure of the rotation rate of the APHID. Although the two-ring APHID was found to be not very rotation sensitive, we believe APHIDs are worthy of further study as multi-ring APHIDs will display enhanced sensitivity to the relative phase between the rings hence potentially leading to increased rotation sensitivity. We shall be exploring multi-ring APHIDs in future research.

This work was supported by the Office of Naval Research Contract No. N00014-99-1-0806, the U.S. Army Research Office, and the Royal Society of Edinburgh. KD acknowledges the support of the UK Engineering and Physical Sciences Research Council.

* ewan.wright@optics.arizona.edu

- [1] L. Deng *et al.*, *Nature* **398**, 218 (1999).
- [2] S. Burger *et al.*, *Phys. Rev. Lett.* **83**, 5198(1999); J. Denschlag *et al.*, *Science* **287**, 97 (2000).
- [3] K. E. Strecker *et al.*, *Nature* **417**, 150(2002).
- [4] M. R. Matthews *et al.*, *Phys. Rev. Lett.* **83**, (1999); K. W. Madison *et al.*, *Phys. Rev. Lett.* **84**, 806 (2000).
- [5] J. Tempere, J. T. Devreese, and E. R. I Abraham, *Phys. Rev. A* **64**, 023603 (2001).
- [6] D.R. Tilley and J. Tilley, *Superfluidity and Superconductivity*, (Adam Hilger Ltd., Bristol 1986), 2nd Edition, Chap. 7.
- [7] J. Javanainen, *Phys. Rev. Lett.* **57**, 3164 (1986).
- [8] E. M. Lifshitz and L. P. Pitaevskii, *Statistical Physics, Part 2* (Pergamon Press, Oxford, 1989) pp. 85-118.
- [9] D. S. Rokhsar, "Dilute Bose gas on a torus: vortices and persistent currents" cond-mat/9709212 (1997).
- [10] J. Javanainen, S. M. Paik, and S. M. Yoo, *Phys. Rev. A* **58**, 580 (1998).
- [11] M. Benakli *et al.*, *Europhys. Lett.* **46**, 275 (1999).
- [12] J. E. Zimmerman, *J. Appl. Phys.* **41**, 1589 (1970).
- [13] W.P. Reinhardt and C.W. Clark, *J. Phys. B: At. Mol. Opt. Phys.* **30**, L785 (1997).
- [14] R. Dum *et al.*, *Phys. Rev. Lett.* **80**, 2972 (1998).
- [15] T.F. Scott, R.J. Ballagh, and K. Burnett, *J. Phys. B: At. Mol. Opt. Phys.* **31**, L329 (1998).
- [16] A.D. Jackson, G.M. Kavoulakis, and C.J. Pethick, *Phys. Rev. A* **58**, 2417 (1998).
- [17] A.E. Muryshev *et al.*, *Phys. Rev. A* **60**, R2665 (1999).
- [18] L. D. Carr *et al.*, *Phys. Rev. A* **62**, 063610 (2000).
- [19] C. Trueman and K. K. Wan, *J. Math. Phys.* **41**, 195 (2000).
- [20] J. A. Fleck, J. R. Morris, and M. D. Feit, *Appl. Opt.* **10**, 129 (1976).
- [21] J. Brand and W. P. Reinhardt, *J Phys. B: At. Mol. Phys.* **34** L113 (2001).
- [22] J. A. Sauer, M. D. Barrett, and M. S. Chapman, *Phys. Rev. Lett.* **87**, 270401 (2001).
- [23] A. S. Arnold and E. Riis, *J. Mod. Opt.* **49**, 959 (2002).
- [24] D. M. Stamper-Kurn *et al.*, *Phys. Rev. Lett.* **80**, 2027 (1998).
- [25] L. Salasnich, A. Parola, and L. Reatto, *Phys. Rev. A* **59**, 2990 (1999).
- [26] E. M. Wright, J. Arlt, and K. Dholakia, *Phys. Rev. A* **63**, 013608 (2000).
- [27] Dallin S. Durfee, Ph. D thesis, *Dynamic properties of dilute Bose-Einstein condensates*, (MIT, 1999).
- [28] T. Freearge and K. Dholakia, *Opt. Commun.* **201**, 99 (2002).
- [29] M. Olshanii, *Phys. Rev. Lett.* **81**, 938 (1998).
- [30] D. S. Petrov, G. V. Shlyapnikov, and J. T. M. Walraven, *Phys. Rev. Lett.* **85**, 3745 (2000).